J Wood Sci (2011) 57:470–478
DOI 10.1007/s10086-011-1202-1

ORIGINAL ARTICLE

Weidong Cheng · Xueqing Xing · Dehong Wang
Kunhao Zhang · Quan Cai · Guang Mo
Zhongjun Chen · Zhonghua Wu

Small-angle X-ray scattering study on nanostructural changes with water content in red pine, American pine, and white ash

Received: October 25, 2010 / Accepted: May 18, 2011 / Published online: August 7, 2011

Abstract Wood is a highly sophisticated and multihierarchical material. The nanoscale structures in natural cell walls of red pine, American pine, and white ash specimens were investigated using the small-angle X-ray scattering (SAXS) technique. A tangent-by-tangent method was used to analyze the SAXS data. The results demonstrate that the multihierarchical scatterers in the three specimens can be divided into two dominant components, i.e., a sharp component and a wide component. The sharp component mainly corresponds to the contribution of cellulose microfibrils, and its size is almost unaffected by the water content. However, the wide component includes voids or microcracks and cellulose microfibril aggregates; its size changes, reflecting swelling and water accumulation in the voids or microcracks. Because of the different morphological features of the cell walls, softwood (red pine and American pine) displays different tendencies from hardwood (white ash) in terms of changes in the wide component with water content: the average scatterer size of the wide component has an incremental tendency with the water content in softwood, but it has a descending tendency in hardwood. Fractal analysis further revealed that in white ash the surface of scatterers is coarser and the scatterers form more compact nanostructures than in the two pine woods. All this nanostructural information can be used to explain well the difference of swelling behaviors between the two pines and the white ash.

Key words Small-angle X-ray scattering · Nanostructure · Water content · Wood

W. Cheng · X. Xing · D. Wang · K. Zhang · Q. Cai · G. Mo · Z. Chen · Z. Wu (✉)
Beijing Synchrotron Radiation Facility, Institute of High Energy Physics, Chinese Academy of Sciences, PO Box 918, Bin 2-7, Beijing 100049, P. R. China
Tel. +86-10-88235982; Fax +86-10-88235982
e-mail: wuzh@ihep.ac.cn

W. Cheng · X. Xing · D. Wang · K. Zhang
Graduate University of Chinese Academy of Sciences, Beijing 100049, P. R. China

Introduction

It is well known that natural wood is a highly sophisticated and multihierarchical material. There are four distinct length scales of hierarchical ordering, i.e., the macroscopic level of tissue structure, the microscopic level of cell structure, the submicroscopic level of cell-wall organization, and the nanoscopic level of cell-wall polymer assembly. The cell wall is a laminated structure in which the thickest S_2 layer occupies 70%–80% of the volume of the cell wall. Due to the hygroscopic property of wood materials, their changes in microstructure with water content are of great interest. It is known that absorbed moisture will cause macroscopically perceptible changes of wood materials, such as swelling[1] or decay.[2] However, the water-absorbing process is mostly associated with the ultrastructure and nanostructure in the texture of wood. Clarifying the nanostructures in wood and their changes with water content is very important in industrial and environmental applications of wood materials.

There have been a number of studies[3–12] about the microstructural changes in wood with water content, but the conclusions on water storage and transport in woods are inconsistent. Christensen[13] pointed out that the uptake of water by plants involves two stages: wetting at capillary surfaces followed by molecular penetration and swelling of the solid phase. Simonaho[14] observed the influence of tap water on the cell wall and cavities of Scots pine, and found that the added water was located inside the cell wall matrix and caused macroscopic swelling of the timber sample. Several research groups[15–17] thought that wood eventually reaches an equilibrium state when the moisture content in wood increased continually, and the cell walls cease further swelling as liquid water begins to accumulate in the lumens and voids. Stamm[18] claimed that the absorbed water was inaccessible to the interior of the cellulose crystallites of the cell wall and was only confined in the amorphous regions or the surface of cellulose crystallites. The imbibition[16,19] of water in wood was found to push apart the polysaccharide molecules. Ma and Rudolph[20] concluded that the main

contributors to water adsorption were the hydroxyl groups of the carbohydrates from cellulose and hemicelluloses in cell walls. Berry and Roderick[15] and Deshpande et al.[21] reported that much of the water in wood was held in the S2 layer and tracheids. Kang and Chung[22] investigated water transport in wood specimens and found that most species had unimodal pore distributions; however, aspen had a bimodal pore distribution. Recent research[23] obtained the nanocrystallite deformation of cellulose microfibrils in spruce wood on dehydration and rehydration. Although all these previous studies are very helpful in understanding the water-absorbing process and the nanostructural changes with water content in wood, due to the structural complexity of wood and possible species differences, the swelling mechanism of wood is still ambiguous, and information about the nanostructural changes in wood with water content is still scarce. More studies are necessary for an unambiguous "image" of water-absorption and water-transport processes in wood.

Usually, absorbed water in wood is in three possible states: as vapor in the gas-filled voids, as free or bulk water in the voids, and as bound water in the cell wall matrix. The absorption of water in wood causes nanoscale electron-density changes. The small-angle X-ray scattering (SAXS) technique[24,25] is quite suitable for the nondestructive study of nanoscale structures. For example, SAXS has been successfully employed to investigate the nanostructure[26–29] in the natural wood cell of *Picea abies*. The nanopore contribution was successfully separated from the cell wall matrix with SAXS data analysis. Cellulose microfibrils (CMFs) of *Picea abies* were confirmed to exist with a uniform fibril diameter only, but the diameters of CMFs obtained by different research groups range approximately from 2 to 4 nm, and the structure function describing the relative arrangement of the cellulose fibers was obtained for the native cell wall. The scanning SAXS[30] technique was also successfully used to identify the fiber direction and size. In this article, SAXS is used to detect the scatterer sizes and their nanostructural evolution with water content in native red pine (*Pinus koraiensis*), American pine (*Pinus elliottii*), and white ash (*Fraxinus americana*). We hope that this study helps elucidate the swelling mechanism and the nanostructural differences between softwood (red pine, American pine) and hardwood (white ash).

Experiments and methods

Three types of wood specimens (native red pine, American pine, and white ash) were carefully prepared for SAXS measurements. For all three species, samples were cut out from the sapwood at breast height without resin canals or knots. The dimensions of the samples were approximately 20 mm in the tangential direction, 30 mm in the longitudinal direction, and 1.5 mm in the radial direction. Each sample had an apparent volume of $V_0 = 0.9 \pm 0.04$ cm^3. These slices were taken from a single annual ring consisting of earlywood and latewood, but the samplings were consciously approximated to the earlywood region of the annual ring. A schematic of the sampling and the wood specimen is shown in Fig. 1. For each wood type, one slice was cut out in the same way. The three wood samples were polished with 1000-mesh sandpaper without chemical treatment and then were washed with deionized water. Finally, these specimens were kept in a desiccator at 150°C and dried until the weight was constant. In our wood slices, the CMFs in the S_2 wall were approximately parallel to the longitudinal direction of the stems.

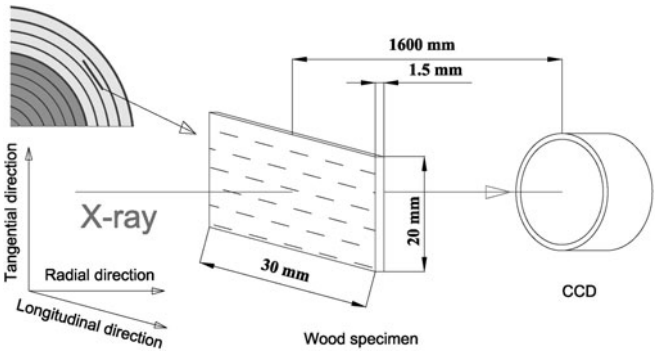

Fig. 1. Schematic of wood samplings and small-angle X-ray scattering (SAXS) measurements. *CCD*, charge-coupled device

Deionized water was directly added to the specimen surfaces by using a Gilson pipette with scale of 0–100 µl. Water addition was controlled and accumulated to 0.04, 0.12, 0.20, 028, 0.36, 0.44, 0.60, and 0.68 ml. At the same time, the water was uniformly dropped on the samples and then spread onto the whole surface. In order to add more water into the specimens, the red pine and white ash specimens were also immersed into the deionized water for 7, 20, 30, 45, and 65 min. Then these specimens were enwrapped with impermeable polyethylene film and closed in vessels for water homogenization in the specimens and to prevent the water from volatilization. About 15 min later, the possible excess water on the specimen surface was removed with filter paper. Before SAXS measurements, the water contents absorbed by the specimens were evaluated by comparing the specimen weight after and before adding water with a Mettler Toledo XS205 electronic balance with an accuracy of 10 µg. The relative volume percentage of moisture in the specimen was given by the formula: $x = V/V_0 = m/V_0$, where $V = m/\rho$, is the volume of absorbed water, m is the weight of the absorbed water, and $\rho = 1$ g/cm^3, the mass density of water.

Because the water was directly added to the surface of the specimens, the moisture distribution in the radial direction (i.e., the thickness direction) of specimens cannot be homogeneous initially. From the surface to the specimen center, a gradient distribution of water content is present. This unevenness of moisture in the sample thickness is the main source of experimental error. If the homogenization time is sufficient, a homogeneous moisture distribution in the thickness direction of the specimens will hopefully be achieved. In our experiments, the exact distribution of water in the specimens was unknown. Moisture distributions[12,16]

have been researched for Scots pines and Norway spruce. It was found that moisture distribution was uneven along the direction of sample thickness after short-term free water soaking, but a flat gradient of moisture distribution was obtained when the sample was immersed in water for 4 h. That is to say, the moisture distribution was approximately uniform in the plane perpendicular to the thickness direction. Therefore, the unevenness of moisture in these planes perpendicular to the incident X-ray direction can be omitted in our samples, because the incident X-ray spot is much smaller than the specimen surface area. Before each SAXS measurement, specimen homogenization was carried out for at least 15 min. From adding water to the specimen to finishing all SAXS measurements with different water contents took a few hours. Therefore, the specimens were in a nonequilibrium state.

The SAXS patterns of the specimens with different water contents were collected using beam line 1W2A of the Beijing Synchrotron Radiation Facility (BSRF) with an incident X-ray wavelength of 0.154 nm. The storage ring was operated at 2.5 GeV with a current of about 200 mA. A Mar 165 two-dimensional charge-coupled device (CCD) detector with 2048×2048 pixels was positioned perpendicularly to the incident beam with a detector–sample distance of 1600 mm, and this was calibrated with a standard sample. During the SAXS measurements, the longitudinal direction of wood growth was placed in the horizontal plane, and the incident X-ray beam was along the radial direction, as shown in Fig. 1. Because SAXS is a statistical average method over the irradiated volume of specimens, one SAXS pattern for each scattering experiment at a specified moisture content was enough to get the statistical average information for nanoscale scatterers. These measured SAXS patterns were firstly transformed into one-dimensional SAXS curves with the software Fit2D.[31] After removal of the instrumental background, the SAXS intensities were normalized to the primary beam intensity.

Results and discussion

As examples, the SAXS patterns of American pine in the dried state and in the hygroscopic state with a volume percentage of moisture of 18.4% are, respectively, shown in Fig. 2a and Fig. 2b. Clearly, the water-absorbed sample has a wider SAXS intensity distribution. Without further SAXS data analysis, it can be concluded that the scatterer sizes in the wood specimens change with the absorbed water content. Figure 2 shows clearly that both SAXS patterns have a double-wedge shape. Similar SAXS patterns were also found for the other wood specimens. As expected, these SAXS patterns imply that the wood material is anisotropic, and the longitudinal direction has a larger particle size than the tangential direction.

According to the specimen orientation, the SAXS signal recorded in the vertical direction of the detector reflects structural information of the tangential direction of the wood specimens. In order to ascertain the scatterer size and distribution, the SAXS data were analyzed using the model-independent tangent-by-tangent (TBT)[32–34] method, which has been successfully applied to decompose the contributions of nanoparticles with different sizes. For a polydisperse particle system, the SAXS intensity with Guinier approximation can be described as:

$$I(q) = I_e \int_0^\infty N(R_g)\rho^2 V^2(R_g) e^{-q^2 R_g^2/3} dR_g \quad (1)$$

where $q = 4\lambda \sin\theta/\lambda$, θ is half the scattering angle, λ is the incident X-ray wavelength, R_g, N, V, and ρ are the radius of gyration, the number of particles with R_g, the volume of a particle with R_g, and the electron density, respectively. I_e is the scattering intensity of one electron. For a system with only a few discrete particle sizes, the integral in Eq. 1 can be discretized as the following summation:

$$I(q) = I_e N_1 n_1^2 e^{-q^2 R_1^2/3} + I_e N_2 n_2^2 e^{-q^2 R_2^2/3} + \cdots + I_e N_i n_i^2 e^{-q^2 R_i^2/3} \quad (2)$$

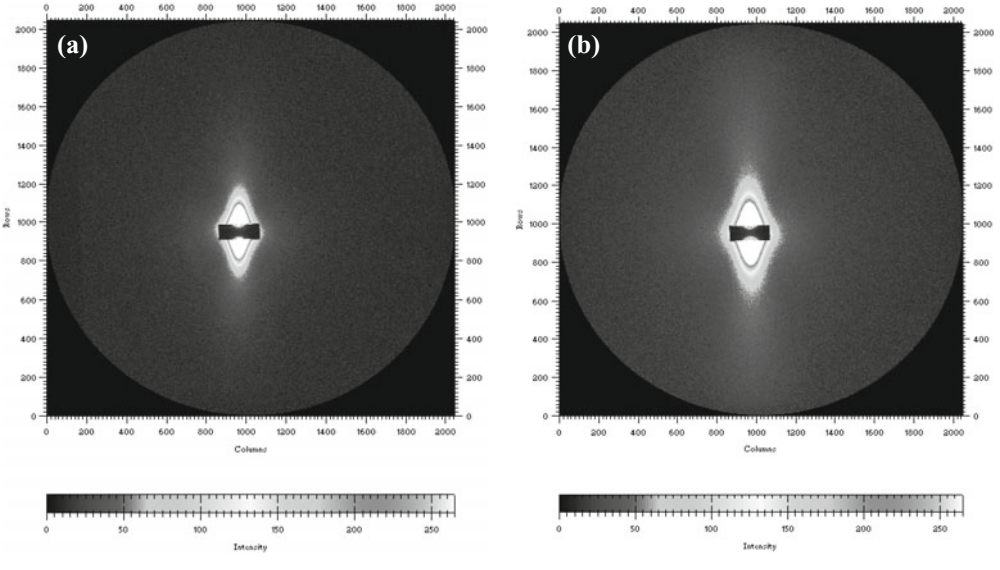

Fig. 2. Two-dimensional SAXS patterns of American pine in the dry state (**a**) and in the hygroscopic state with a volume percentage of moisture of 18.4% (**b**)

where i represents the ith size level. n_i is the electron number in the particle with gyration radius R_i. When $q = 0$, the SAXS intensity is given as:

$$I(0) = K_1 + K_2 + \cdots + K_i \tag{3}$$

where $K_i = I_e N_i n_i^2 = I_e N_i \rho^2 V_i^2 = I_e \rho^2 N_i V_i V_i = I_e \rho^2 W_i c R_i^3$ is the intercept of the ith tangent on the ordinate. The gyration radius R_i can be obtained from the slope of the ith tangent. Therefore, the volume percentage is given by:

$$W_1 : W_2 : \cdots : W_i = \frac{K_1}{R_1^3} : \frac{K_2}{R_2^3} : \cdots : \frac{K_i}{R_i^3} \tag{4}$$

The experimental SAXS intensities and the values calculated using the TBT method are shown in Figs. 3a, 3b, and 3c, respectively, for the red pine, American pine, and white ash specimens. The SAXS fitting curves are all in excellent agreement with the experimental data. The normalized volume fractions (NVFs) were obtained for the three wood specimens, as shown in Fig. 4. Each of the NVFs of the three wood specimens can be divided into two distinct parts: a sharp component (feature C) with a smaller particle size and a wide component (dominant features A and B) with a larger particle size.

In the three wood specimens, feature C is less changeable with variation of the volume percentage of moisture. The most probable values of the gyration radius R_g are, respectively, 1.1, 1.1, and 1.2 nm, with slight fluctuations, for the sharp components in red pine, American pine, and white ash specimens. The average values of the sharp components are, respectively, around 2.3 ± 0.4, 2.2 ± 0.3, and 2.2 ± 0.6 nm for the red pine, American pine, and white ash specimens. Evidently, even for the sharp components, the respective scatterer size is also not a single value for the three specimens.

It is well known that the nanoscopic cell-wall polymer assembly consists of CMFs, amorphous hemicellulose, and lignin. The CMFs of wood specimens are anisotropic and can be approximately described as cylindrical scatterers. Their axial direction is along the longitudinal direction, and their radial direction is perpendicular to the longitudinal direction. According to the orientation of specimens relative to the incident X-ray beam, a wafer model can be used to evaluate the diameter of the cylindrical scatterers. The physical diameters are obtained as 3.1, 3.1, and 3.4 nm for the most probable contribution of the sharp components in red pine, American pine, and white ash specimens, respectively. These values are in excellent agreement with the sizes[21,27] of CMFs in previous reports. Therefore, we can attribute feature C to the contribution of CMFs and can conclude that the size of CMFs is approximately unchangeable with the volume percentage of moisture. This result demonstrates that the water-absorbing process or the increase of the volume percentage of moisture does not alter the size of CMFs in the three wood specimens studied. In other words, there is almost no interaction between water molecules and cellulose molecules inside CMFs. This conclusion confirms the findings of a previous report[18] that water molecules could not enter the interior of CMF crystallites. However, CMFs can aggregate into larger structural

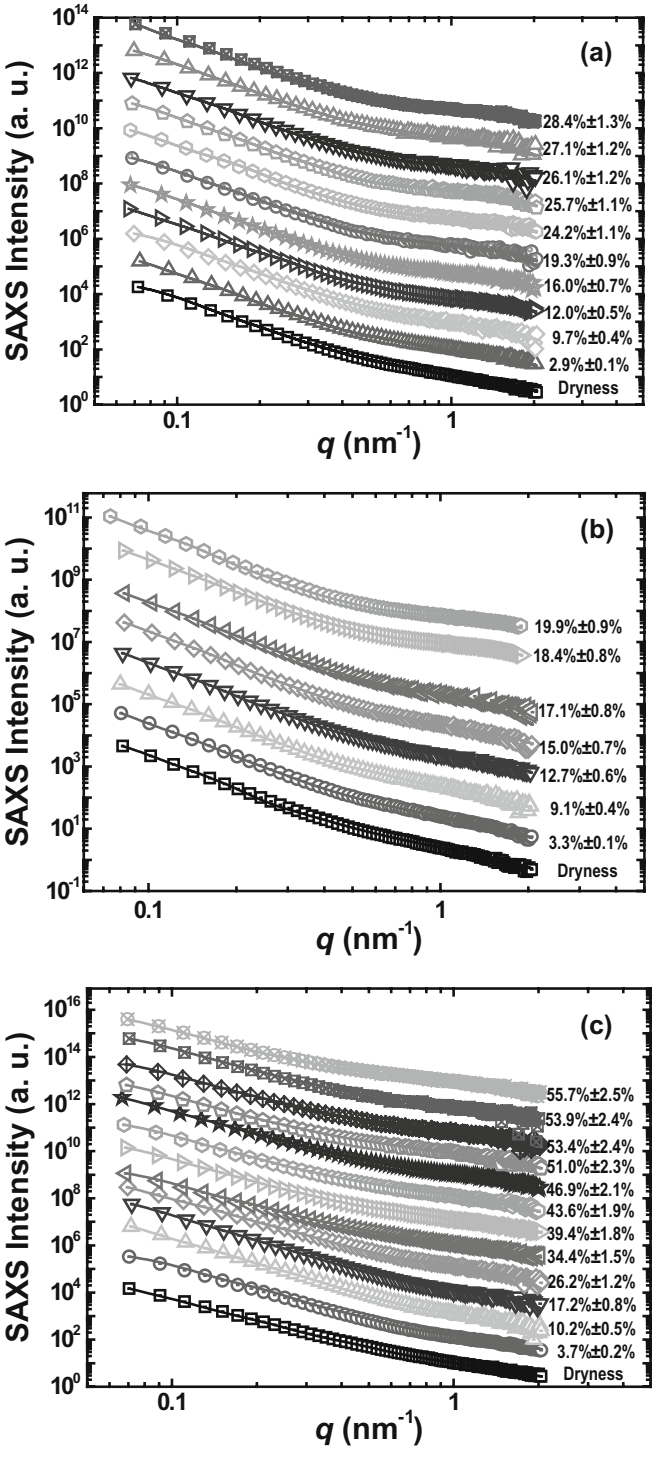

Fig. 3a–c. Comparison between the experimental SAXS intensities (*symbols*) and the calculated values (*solid lines*). **a** The red pine specimen. From bottom to top, the volume percentages (V/V_0) of absorbed water are 0%, 2.9%, 9.7%, 12.0%, 16.0%, 19.3%, 24.2%, 25.7%, 26.1%, 27.1%, and 28.4%. **b** The American pine specimen. From bottom to top, the volume percentages (V/V_0) of absorbed water are 0%, 3.3%, 9.1%, 12.7%, 15.0%, 17.1%, 18.4%, and 19.9%. **c** The white ash specimen. From bottom to top, the volume percentages (V/V_0) of absorbed water are 0%, 3.7%, 10.2%, 17.2%, 26.2%, 34.4%, 39.4%, 43.6%, 49.6%, 51.0%, 53.4%, 53.9%, and 55.7%. The SAXS curves are offset in vertical direction for clarity

units[21,35–37] with a diameter of about 7–30 nm. Terashima et al.[38] also suggested that the cross section of the composite unit [CMF bundle + hemicellulose–lignin module] was square with a side of 18 ± 1 nm, with a possible parallelogramic or hexagonal cross section of a bundle of CMFs of 12 ± 3 nm across. In addition, there were also some molecule-scale cavities and voids[15,25,27] in the hemicellulose–lignin matrix, which could divide the cell wall into smaller regions. It is these smaller regions and the smaller CMF aggregations that can contribute partially to the sharp components of the three wood specimens, which results in an asymmetrical distribution in the NVFs of the sharp components.

The wider components in the NVFs of the three wood specimens are variable. The much wider distribution of scatterer sizes can be attributed to the contribution of polydisperse scatterer sizes (for example, the possible voids or microcracks as well as the CMF aggregates) and the gradient distribution of moisture. Features A and B belong to the wide component. They are, respectively, located at 17.8 nm and 9.4 nm for the initial state (dryness) of the white ash specimen, 15.8 nm and 6.4 nm in the initial state of the American pine specimen, and 14.8 nm and 8.8 nm in the initial state of the red pine specimen. The large difference of gyration radii between features A and B cannot be attributed to the swelling difference in the specimen thickness because the gradient of moisture is approximately continuous[39] in the thickness direction of specimens. Thus, two distinct gyration radii within the wide component illustrate that a multimodal size distribution exists in the three wood specimens. This result is not in agreement with previous research[22] by Kang and Chung who claimed that most species had unimodal pore distributions, except for aspen, which had a bimodal pore distribution. The changes of gyration radii R_g of features A and B with water content (bottom abscissa) or volume percentage of moisture (top abscissa) are shown in the insets of Fig. 4. In general, the sizes of features A and B increase with increasing water content, presenting a swelling behavior versus volume percentage of moisture. Based on the most probable sizes of features A and B, a reasonable conjecture is that features A and B contain, respectively, the contribution of the CMF bundles and the surrounding tubular hemicellulose–lignin matrix (HLM). Under the infinite cylinder hypothesis, the physical diameters of CMF bundles are, respectively, about 25, 22, and 21 nm for white ash, American pine, and red pine, and the corresponding thicknesses of HLM are, respectively, about 13, 9, and 12 nm. These values are approximately twice those of Terashima's model.[38]

The initial average sizes of the detectable scatterers in the wide components are estimated to be 40 ± 3, 41 ± 2, and 38 ± 2 nm for the dry states of red pine, American pine, and white ash specimens, respectively. Evidently, the wide components not only contain the contribution of CMF bundles and HLM, but also contain other scatterers, such as voids or microcracks, or even the lumens. Nanocrystallite deformation of CMFs in the S2 layer of spruce wood tracheids was observed[23] during dehydration and rehydration experiments below the fiber saturation point. It was the removal

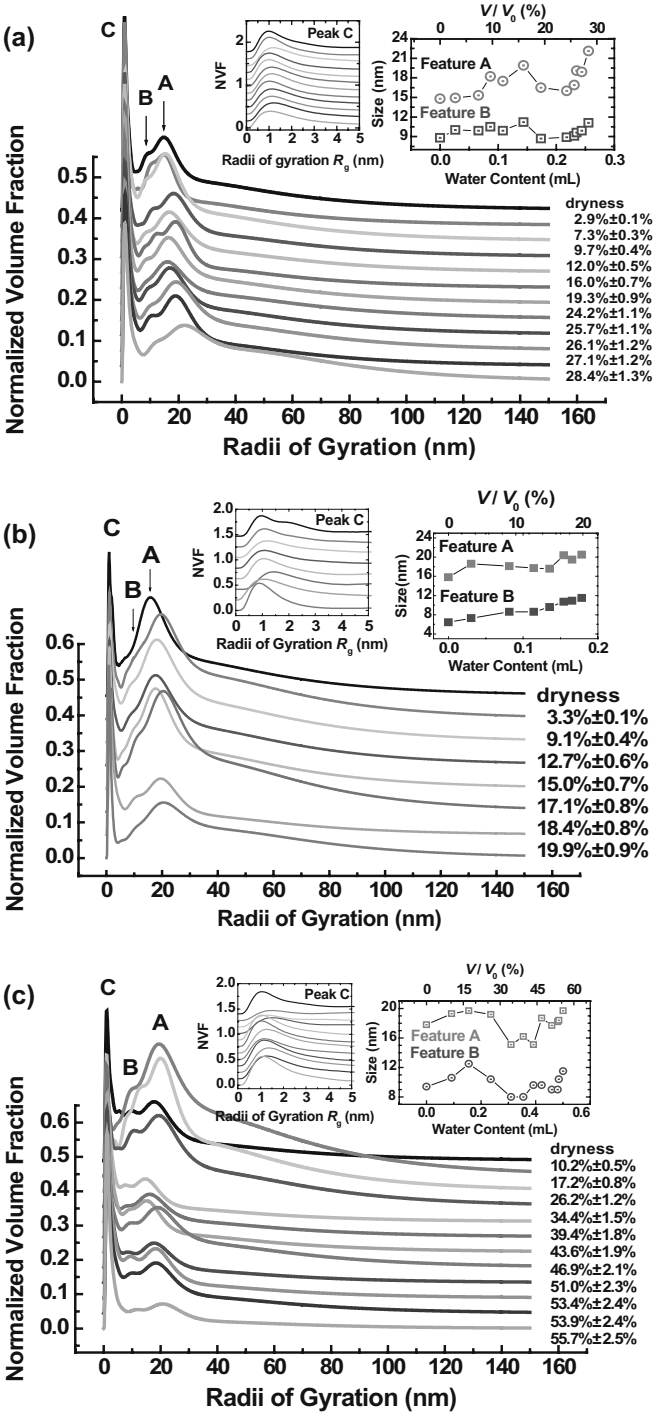

Fig. 4a–c. Normalized volume fraction of scatterers. **a** The red pine specimen. From top to bottom, the volume percentages (V/V_0) of absorbed water are 0%, 2.9%, 7.3%, 9.7%, 12.0%, 16.0%, 19.3%, 24.2%, 25.7%, 26.1%, 27.1%, and 28.4%. **b** The American pine specimen. From top to bottom, the volume percentages (V/V_0) of absorbed water are 0%, 3.3%, 9.1%, 12.7%, 15.0%, 17.1%, 18.4%, and 19.9%. **c** The white ash specimen. From top to bottom, the volume percentages (V/V_0) of absorbed water are 0%, 10.2%, 17.2%, 26.2%, 34.4%, 39.4%, 43.6%, 46.9%, 51.0%, 53.4%, 53.9%, and 55.7%. The insets enlarge feature C or show the size evolutions of feature A and feature B with the water content (*bottom abscissa*) or the volume percentage (*top abscissa*)

of the extra water that created enormous stresses in the cell wall and caused longitudinal contraction, lateral expansion, and changes in the monoclinic angle of the cellulose unit cell during drying of wood fibres. Because the whole cell wall material is destabilized when drying wood beyond the fiber saturation point, some voids or microcracks with larger sizes can be formed and contribute to the wide component.

We also noted the following variational tendency of features A and B. At first, the sizes of features A and B increase with the volume percentage of moisture; however, as the water content in the specimens reaches certain values, the sizes of features A and B begin to decrease. With further increase of water content, the sizes of features A and B increase again. From Figs. 4a and 4c, it can be found that there is size "shrinkage" in features A and B when the volume percentage of moisture is around 23% for the red pine specimen, or is around 35% for the white ash specimen. An explanation for this phenomenon is that when water penetrates into a wood specimen, a small quantity of water is stored in the cell wall matrix. With the increase of water in the specimens, liquid water begins to accumulate in the lumens and voids or microcracks. At this stage, the nanoscale voids or microcracks gradually fill with water. Therefore, the average size of scatterers (liquid water and the unfilled portions of the voids) with respective uniform electron density would first decrease and then increase, presenting a concave-down feature in the curve of scatterer size versus volume percentage of moisture, as shown in the insets of Figs. 4a and 4c. In this case, the size "shrinkage" of features A and B does not mean that the wood specimens were contracting in the water-absorbing process. It is simply the cumulative progress of water in the nanoscale voids or microcracks and lumens. The volume percentage of moisture related to the "shrinkage" is larger in white ash (~35%) than in red pine (~23%). Red pine and white ash can be classified as softwood and hardwood, respectively. Usually, softwoods have thinner cell walls and larger lumens, while hardwoods have thicker cell walls and narrower lumens. Before the water accumulates in the lumens and voids, the thicker cell wall can hold more water in the initial water-absorbing process so that the "shrinkage" occurs at a larger volume percentage of moisture in white ash than in red pine.

Figure 5 illustrates the evolutionary processes of the average R_g versus the absorbed water content (bottom abscissa) or the volume percentage of moisture (top abscissa). In the cases of the red pine and the American pine specimens, the R_g of the sharp component is almost unchanged with the absorbed water content, but the R_g of the wide component increases slightly with the volume percentage of moisture. However, in contrast to the red pine and American pine specimens, the white ash specimen has a faster increase in average R_g of the sharp component with water content. Also, the average R_g of the wide component shows a decreasing tendency with the volume percentage of moisture. These different characteristics of the average R_g versus water content can be ascribed to the different nanostructures in red pine, American pine, and white ash. Both pine specimens are softwoods; they have cells with an

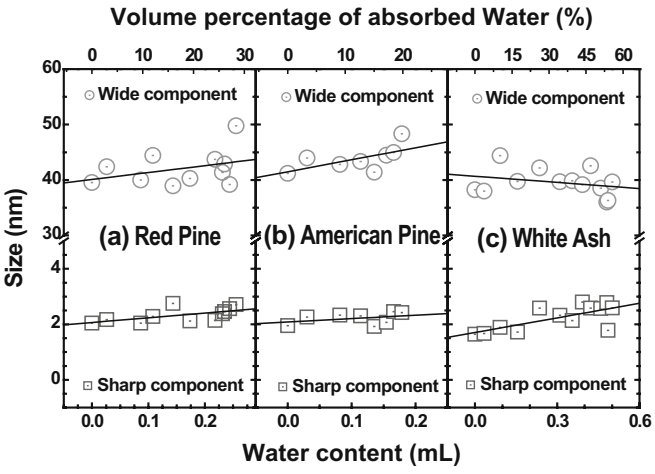

Fig. 5. Average radii of gyration changes with the water content (*bottom abscissa*) or the volume percentage of absorbed water in the specimens (*top abscissa*) for the sharp component (*squares*) and the wide component (*circles*) in the red pine specimen (**a**), the American pine specimen (**b**), and the white ash specimen (**c**). *Lines* are the linear best fit values

open lumen and thinner cell walls. In contrast, the white ash specimen is a hardwood; its cells are thick-walled with a narrower central lumen. In addition, the nanostructure in the white ash is more compact, which creates better strength and bending tenacity compared with the pine wood. For the softwoods (red pine and American pine), the absorbed water exists mainly in the nanoscale voids or microcracks of cell walls and the larger lumen. Because the cell wall is thinner and with looser structures, the swelling, including the expansion of nanoscale voids or microcracks, makes less contribution to the sharp component, which results in the relatively constant R_g of the sharp component. At the same time, the expansion of the lumen and voids or microcracks can cause the increasing R_g of the wider component. But in hardwood (white ash), more water enters the amorphous hemicellulose and lignin surrounding CMFs. Because of the thicker cell wall and the more compact structures, the swelling of cell walls and the expansion of nanoscale voids or microcracks make a larger contribution to the sharp component. Some small amount of water formed at the cell wall will contribute partially to the sharp component, causing an increase of average R_g of the sharp component. Simultaneously, the swelling of the thicker cell walls probably invades the volume of the central lumen (including the voids or microcracks) so that the size of the wider component decreases with the volume percentage of moisture. We believe that the size of water droplets formed in the lumens increases with the increase of water content. Thus, it is the difference of nanostructures between pines and white ash that leads to different trends in average R_g, as shown in Fig. 5.

From the above analysis, we confirmed that the water content has a prominent influence on the size changes of features A and B, which correspond to the contribution of CMF aggregates, voids or microcracks, and water droplets

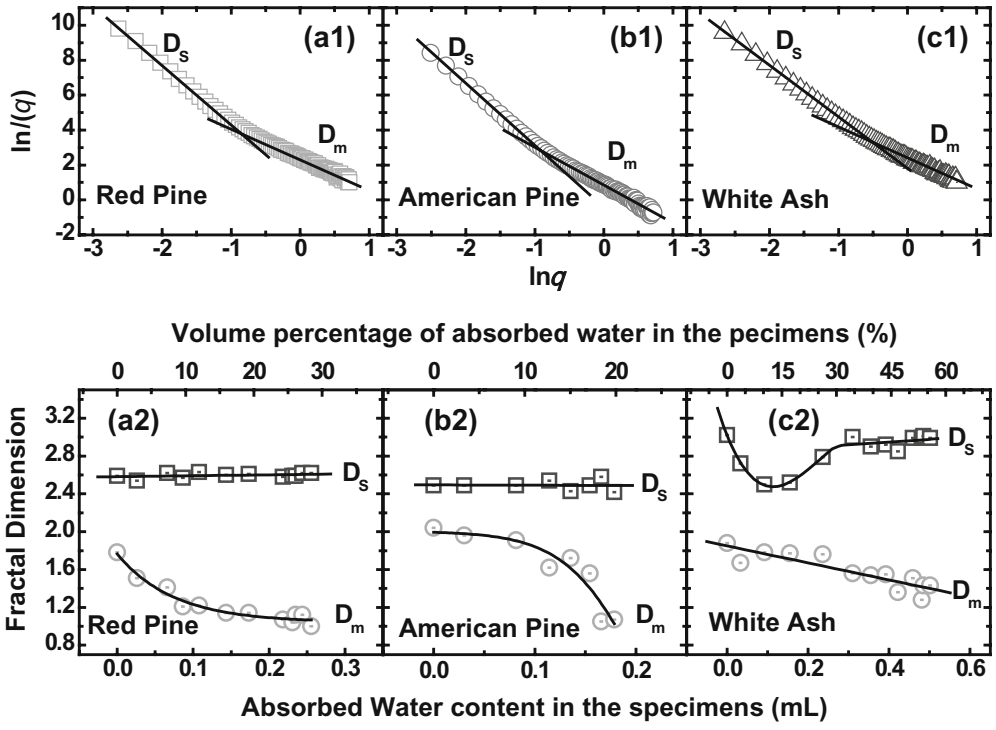

Fig. 6. Mass fractal dimension (D_m) and surface fractal dimension (D_s). The ln$I(q)$ vs. ln$q$ plots show the experimental SAXS intensities (*symbols*) and the linear best fit values (*lines*) for red pine (**a1**), American pine (**b1**), and white ash (**c1**) specimens in the dry state. The changes of D_m and D_s with water content (*bottom abscissa*) or the volume percentage of absorbed water in the specimens (*top abscissa*) are shown for red pine (**a2**), American pine (**b2**), and white ash (**c2**)

in the interior of lumens. For these detectable scatterers in the wider component, the average sizes over specimens with different water contents were estimated to be 42 ± 4, 44 ± 3, and 40 ± 3 nm; the standard deviations of the regression lines were 3, 2, and 2 nm for red pine, American pine, and white ash, respectively. Although softwood (red pine and American pine) has a larger swelling rate than hardwood (white ash), the average sizes of scatterers in the wide component over the water-absorption process hardly change, if considering the standard deviation; however, the change tendencies of the regression lines are still credible.

It is well known that more voids and cavities are produced[40] with the increase of water uptake. On the basis of Fig. 5, we can conclude that the swelling of softwood (red pine and American pine) is mainly dependent on the expansion of voids or microcracks and water droplet size in lumens with the volume percentage of moisture, which leads to more marked swelling behavior. However, hardwood, for example white ash, has a more compact structure and thicker cell walls. Its swelling depends mainly on the expansion of cell walls with the volume percentage of moisture. The compression of the larger lumens compensates partially the swelling of the amorphous hemicellulose and lignin in the cell wall. As a result, white ash presents a lower swelling value. These behaviors are consistent with the swelling phenomena of softwood and hardwood.

In addition to the radius of gyration, fractal dimension[41,42] is also a crucial parameter to describe nanoscale structures. SAXS data can be employed to analyze the fractal structure. The fractal dimension D is just used to quantify the changes of the mass or the surface of scatterers. In such a case, the SAXS intensity can be described as:

$$I(q) = Cq^{-\alpha} \tag{5}$$

where C is a constant. The coefficient α can be obtained from the plot of $\ln I(q)$ vs. $\ln q$. For a mass fractal: $1 \le \alpha < 3$, and the mass fractal dimension $D_m = \alpha$. For a surface fractal: $3 \le \alpha < 4$, and the surface fractal dimension $D_s = 6 - \alpha$. D_s reveals the roughness of the scatterer surface. The bigger the D_s value is, the coarser the surface. D_m displays the compactness of the scatterer. The smaller the D_m value is, the looser the structure. The fractal dimensions as a function of absorbed water contents (bottom abscissa) or volume percentage of moisture (top abscissa) are shown in Fig. 6. It can be seen that mass fractal and surface fractal coexist in the three wood specimens. Although the mass fractal dimensions D_m always decreases with an increase of the absorbed water content, the three wood specimens have different decreasing trends. For softwood, the change of D_m versus water content is nonlinear, but the trend is linear in hardwood. This differences in D_m indicate that the bond force in hardwood is stronger than in softwood. The decreasing tendency of D_m illuminates that the inner structures of the scatterers in the three wood specimens become less compact with increasing water content, which is caused by the swelling of the wood. The surface fractal dimensions D_s are almost unchanged for the red pine and the American pine specimens, demonstrating that the coarseness of the scatterer surface in red pine and American pine does not change with the increasing water content. However, an initial fast decrease is accompanied with a succeeding slow increase in the D_s curve versus water content for the white ash specimen; the transition between the two occurs at a volume moisture percentage of about 11.1%, as shown in Fig. 6c2.

This change implies that the voids or microcracks in white ash specimen have an increasing tendency at the initial stage. Subsequently, the swelling of the cell wall invades partially the volume of the lumen, which causes a compression of the larger voids or microcracks and results in a slow increase of the surface coarseness. The larger D_s values of the white ash specimen indicate that the coarseness of the scatterer surface in the cell walls of white ash is greater than that in the other two specimens. Such a coarse surface might compensate partially the swelling of the wood specimen with the volume percentage of moisture.

The morphological differences of cell wall polymers between softwood and hardwood are mainly focused on the thickness of the cell wall and the lumen size, which reflect the density of wood. Although the three wood specimens all have CMF bundles surrounded by amorphous hemicellulose–lignin matrix (HLM) in the S2 layer of cell walls, the sizes of CMF bundles and the HLM thickness are different. Some molecule-scale cavities exist in the HLM, and nanoscale microcracks exist in the S2 layers of cell walls due to the drying process. Absorbed water can enter these microcracks and the lumens to form water droplets. Some microcracks and the water droplets could be larger than 40 nm. The size of water droplets has an obvious effect on the wide component changes with water content. The morphological features of the cell wall determine the swelling behavior of the wood. However, the nanoscopic morphological features of cell walls could be changed in the drying process of wood due to the weathering of hemicellulose or reannealing of cellulose or the high surface tension of water on CMFs. The rehydration process of dry wood and the dehydration process of green wood are not reversible. That is to say, the water content distribution could be different between the swelling process of dried wood and the drying process of green wood. The difference of nanoscopic characteristics with water content between dehydration and rehydration processes of wood is still ambiguous. Comparing the swelling process of dried wood with the drying process of green wood is worthy of further study in future. It promises to give additional insight into the differences in nanoscopic characteristics between dried samples and never-dried samples.

Conclusions

The nanostructural changes with absorbed water content in red pine, American pine, and white ash specimens were studied using the SAXS technique. The obtained results were compared among the three wood specimens and can be summarized as follows. The nanostructures in the three wood specimens consist of a sharp component and a wide component. The main contribution to the sharp component comes from CMFs, the size of which remain constant (~3 nm) during the whole water-absorbing process. There is no obvious interaction between water molecules and cellulose molecules inside CMFs. The wide component includes voids, microcracks, and CMF aggregates. The size change of the wide scatterer component is related to the swelling behavior. A different nanostructural evolution was found between softwood (red pine and American pine) and hardwood (white ash). In softwood, the size of the wide scatterer component has an incremental tendency with the volume percentage of moisture, but it has a descending tendency in hardwood. The absorbed water exists mainly in the open lumens in softwood, or in the amorphous hemicellulose and lignin surrounding CMFs in hardwood. The surface or interface of the scatterers is coarser in hardwood (white ash) than in softwood (red pine and American pine). Such a coarse surface of scatterers compensates partially the swelling caused by the absorbed water. The structural looseness of the scatterers increases with the increase of the volume percentage of moisture in all three wood species.

Acknowledgments This work was supported by the National Natural Science Foundation of China with Grant Nos. 10374087 and 10835008, the Knowledge Innovation Program of the Chinese Academy of Sciences (Grant No. KJCX3-SYW-N8), and the Momentous Equipment Program of the Chinese Academy of Sciences (Grant No. YZ200829).

References

1. Murata K, Masuda M (2006) Microscopic observation of transverse swelling of latewood tracheid: effect of macroscopic/mesoscopic structure. J Wood Sci 52:283–289
2. Chirkova J, Irbe I, Andersons B, Andersone I (2006) Study of the structure of biodegraded wood using the water vapour sorption method. Int Biodeter Biodegr 58:162–167
3. Ashori A, Sheshmani S (2010) Hybrid composites made from recycled materials: Moisture absorption and thickness swelling behavior. Bioresource Technol 101:4717–4720
4. Berthold J, Rinaudo M, Salmen L (1996) Association of water to polar groups: estimations by an adsorption model for lignocellulose materials. Colloid Surf A: Physicochem Eng Aspects 112:117–129
5. Hartley ID, Kamke FA, Peemoeller H (1992) Cluster theory for water sorption in wood. Wood Sci Technol 26:83–99
6. Oliveira FGR, Candian M, Lucchette FF, Salgon JL, Sales A (2005) A technical note on the relationship between ultrasonic velocity and moisture content of Brazilian hardwood (*Goupia glabra*). Build Environ 40:297–300
7. Qing H, Mishnaevsky L (2009) Moisture-related mechanical properties of softwood: 3D micromechanical modeling. Comput Mater Sci 46:310–320
8. Sadler RL, Sharpe M, Panduranga R, Shivakumar K (2009) Water immersion effect on swelling and compression properties of Eco-core, PVC foam and balsa wood. Compos Struct 90:330–336
9. Simpson WT (1980) Sorption theories applied to wood. Wood Fiber 12:183–195
10. Skaar C (1988) Wood–water relations. Springer-Verlag Berlin, Heidelberg, New York
11. Švedas V (1998) Cellulose-water vapour interaction investigated by spectrometric and ultra-high-frequency methods. J Phys D Appl Phys 31:1752–1756
12. Virta J, Koponen S, Absetz I (2006) Modeling moisture distribution in wooden cladding board as a result of short-term single-sided water soaking. Build Environ 41:1593–1599
13. Christensen GN (1967) Sorption and swelling within wood cell walls. Nature 213:782–784
14. Simonaho SP, Tolonen Y, Rouvinen J, Silvennoinen R (2003) Laser light scattering from wood samples soaked in water or in benzyl benzoate. Optik 114:445–448
15. Berry SL, Roderick ML (2005) Plant-water relations and the fibre saturation point. New Phytol 168:25–37

16. Kouali ME, Vergnaud JM (1991) Modeling the process of absorption and desorption of water above and below the fiber saturation point. Wood Sci Technol 25:327–339
17. Stamm AJ, Petering WH (1940) Treatment of wood with aqueous solution. Ind Eng Chem 32:809–813
18. Stamm AJ (1977) Monomolecular adsorption and crystallite diameters of cellulose from structural and adsorption considerations. Wood Sci Technol 11:39–49
19. Parham RA, Gray RL (1984) Formation and structure of wood. In: The chemistry of solid wood. American Chemical Society, Washington, DC, pp 3–56
20. Ma Q, Rudolph V (2006) Prediction of vapor-moisture equilibriums for a wood-moisture system using a modified UNIQUAC model. Chem Eng Sci 61:6077–6084
21. Deshpande AS, Burgert I, Paris O (2006) Hierarchically structured ceramics by high-precision nanoparticle casting of wood. Small 2:994–998
22. Kang W, Chung WY (2009) Liquid water diffusivity of wood from the capillary pressure-moisture relation. J Wood Sci 55:91–99
23. Zabler S, Paris O, Burgert I, Fratzl P (2010) Moisture changes in the plant cell wall force cellulose crystallites to deform. J Struct Biol 171:133–141
24. Glatter O, Kratky O (1982) Small angle X-ray scattering. Academic Press, New York
25. Jungnikl K, Paris O, Fratzl P, Burgert I (2008) The implication of chemical extraction treatments on the cell wall nanostructure of softwood. Cellulose 15:407–418
26. Jakob HF, Fratzl P, Tschegg SE (1994) Size and arrangement of elementary cellulose fibrils in wood cells: a small-angle X-ray scattering study of *Picea abies*. J Struct Biol 113:13–22
27. Jakob HF, Fengel D, Tschegg SE, Fratzl P (1995) The elementary cellulose fibril in *Picea abies*: comparison of transmission electron microscopy, small-angle X-ray scattering, and wide-angle X-ray scattering results. Macromolecules 28:8782–8787
28. Jakob HF, Fengel D, Tschegg SE, Fratzl P (1996) Hydration dependence of the wood-cell wall structure in *Picea abies*. A small-angle X-ray scattering study. Macromolecules 29:8435–8440
29. Reiterer A, Jakob HF, Stanzl-Tschegg SE, Fratzl P (1998) Spiral angle of elementary cellulose fibrils in cell walls of *Picea abies* determined by small-angle X-ray scattering. Wood Sci Technol 32:335–345
30. Fratzl P, Jakob HF, Rinnerthaler S, Roschger P, Klaushofer K (1997) Position-resolved small-angle X-ray scattering of complex biological materials. J Appl Cryst 30:765–769
31. Hammersley A (1987) Program FIT2D. In: European Synchrotron Radiation Facility, http://www.esrf.eu/computing/scientific/FIT2D. Accessed: May 13, 2011
32. Jellinek MH, Solomon H, Fankuchen I (1946) Measurement and analysis of small-angle X-ray scattering. Ind Eng Chem 18:172–175
33. Jellinek MH, Fankuchen I (1949) X-ray examination of pure alumina gel. Ind Eng Chem 41:2259–2265
34. Wang W, Chen X, Cai Q, Mo G, Jiang LS, Zhang KH, Chen ZJ, Wu ZH, Pan W (2008) In situ SAXS study on size changes of platinum nanoparticles with temperature. Eur Phys J B 65:57–64
35. Fahlén J, Salmén L (2003) Cross-sectional structure of the secondary wall of wood fibers as affected by processing. J Mater Sci 38:119–126
36. Fahlén J, Salmén L (2005) Pore and matrix distribution in the fiber wall revealed by atomic force microscopy and image analysis. Biomacromolecules 6:433–438
37. Zhang YHP, Lynd LR (2004) Toward an aggregated understanding of enzymatic hydrolysis of cellulose: noncomplexed cellulase systems. Biotechnol Bioeng 88:797–824
38. Terashima N, Kitano K, Kojima M, Yoshida M, Yamamoto H, Westermark U (2009) Nanostructural assembly of cellulose, hemicellulose, and lignin in the middle layer of secondary wall of ginkgo tracheid. J Wood Sci 55:409–416
39. Espert A, Vilaplana F, Karlsson S (2004) Comparison of water absorption in natural cellulosic fibres from wood and one-year crops in polypropylene composites and its influence on their mechanical properties. Compos Part A 35:1267–1276
40. Robertson AA (1961) The measurement of fiber flexibility. Pulp Paper Can 62:T3–T10
41. Chattopadhyay S, Erdemir D, Evans JMB, Ilavsky J, Amenitsch H, Segre CU, Myerson AS (2005) SAXS study of the nucleation of glycine crystals from a supersaturated solution. Cryst Growth Des 5:523–527
42. Grigoriew H, Luboradzki R, Cunis S (2004) In situ studies of monosaccharide gelation using the small-angle X-ray scattering time-resolved method. Langmuir 20:7374–7377